ACS APPLIED MATERIALS & INTERFACES

Research Article

www.acsami.org

Encapsulation of Metal Oxide Nanocrystals into Porous Carbon with Ultrahigh Performances in Lithium-Ion Battery

Jun Ming, Jin-Bum Park, and Yang-Kook Sun*

Department of Energy Engineering, Hanyang University, Seoul,133-791, Republic of Korea

Supporting Information

ABSTRACT: A simple and industrial scalable approach was developed to encapsulate metal oxide nanocrystals into porous carbon (PC) with a high distribution. With this method, the composite of PC-metal oxide were prepared in a large amount with a low cost; particularly they exhibit ultrahigh performances in lithium-ion battery applications. For example, the PC-CoO_x and PC-FeO_x show a high capacity around 1021 mA h g^{-1} and 1200 mA h g^{-1} at the current density of 100 mA g^{-1} respectively, together with an excellent cycling ability (>400 cycles) and rate capacity even at the high current densities of 3 A g^{-1} and 5 A g^{-1}.

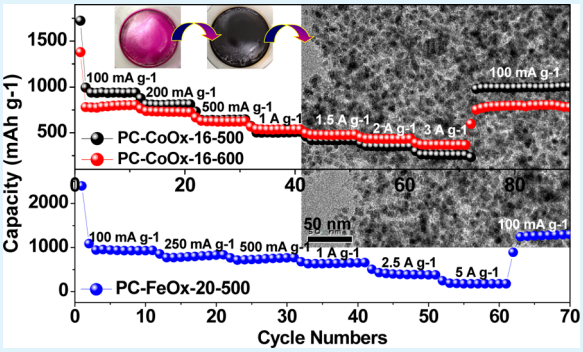

KEYWORDS: *metal oxide, carbon, composite, lithium-ion batteries, anode*

INTRODUCTION

In the past few decades, much effort have been paid on applying the metal oxide as anode materials in lithium-ion battery applications, because its theoretical higher capacity (most >800 mA h g^{-1}) compare to the commercial carbon-based anode (~320 mA h g^{-1}).[1−4] To date, numerous metal oxides, such as SnO_2,[5−7] SiO_x,[8] Fe_2O_3,[9,10] NiO,[11,12] and Co_3O_4,[13,14] are being continually investigated. To enhance their practical capacity, cycling performance, and rate capability of metal oxides, most researchers kept preparing the popular nanosized metal oxide with different morphologies and structures (e.g., nanoparticles,[7,15] hollow spheres,[2,6] arrays,[12] film,[13] etc.), because nanoscale metal oxides often exhibit improved properties compared to bulk ones. Alternatively, many kinds of nanostructured metal oxides were also further coated with a layer of carbon (e.g., SnO_2@C spheres,[16] SiO_x@C[17]), or the oxide-carbon composites (e.g., CuO−CNTs,[18] Fe_3O_4−C,[19] Mn_3O_4−graphene[20]) are being synthesized directly to improve the capacity/cyclability of the oxide.

However, most previous research has had difficulty achieving the goal of practical production even excellent performances were demonstrated, because the method to prepare nanosized oxide and oxide-carbon composites often processed in the solution and remains in an experiential scale. Generally, only a limited amount of products was obtained, let alone complex steps of separation and washing. Recently, the nano/mesoporous materials of carbon, silica, and metal (oxide) have been attracting great attention for their intriguing performances in the widespread fields of catalysis,[21] sensors,[22] and energy and environmental technologies[23,24] because of their rich porosity and large surface area. Herein, we present a simple and industrial-scale way to encapsulate metal oxide nanocrystals into porous carbon (PC) for preparing PC-metal oxide such as PC-CoO_x and PC-FeO_x with ultrahigh performances in the lithium-ion battery application.

EXPERIMENTAL SECTION

12.0 g Pluronic F127 and 16−40 g $Co(NO_3)\cdot 6H_2O$ or 20 g $Fe(NO_3)_3\cdot 9H_2O$ were dissolved in 60 g of ethanol at 40 °C, and then 38.65 g of resol-ethanol (20 wt %) was added into the solution. Keep stirring for 4 h and then transferring them into a dish to evaporate the ethanol in oven. After drying, slowly elevating the temperature to 100 °C for the further polymerization of the resol (Figure 1a, inset), and finally calcination at 450−600 °C for 2 h (2 °C min^{-1}) in Ar gives rise to PC-metal oxide. To facilitate the comparison, the acronym of PC-metal oxide-mass of precursor (g)-calcination temperature (°C) were used, such as MC-CoO_x-16−500. Electrochemical measurement are the same as our recently works.[4] The used electrolyte is 1.0 M $LiPF_6$ in ethylene carbonate/diethyl carbonate (1:1 v/v) and the electrode consist of active materials, PVDF, Super C and KS-6 with a weight ratio of 8:1:0.5:0.5.

RESULTS AND DISCUSSION

Varying the calcination temperature from 450 over 500 to 600 °C, different crystalline structured CoO_x could be obtained, as confirmed by the variation of peaks move around in the comparative X-ray Diffraction (XRD) patterns (Figure 1b). The reason was ascribed to the cobalt oxide, thermal decomposed from $Co(NO_3)_2\cdot 6H_2O$, could react with elements of C, H and O that existed in the resol and F127 during the carbonization. The competitive degree of these redox-oxidation reactions

Received: December 20, 2012
Accepted: February 13, 2013
Published: February 13, 2013

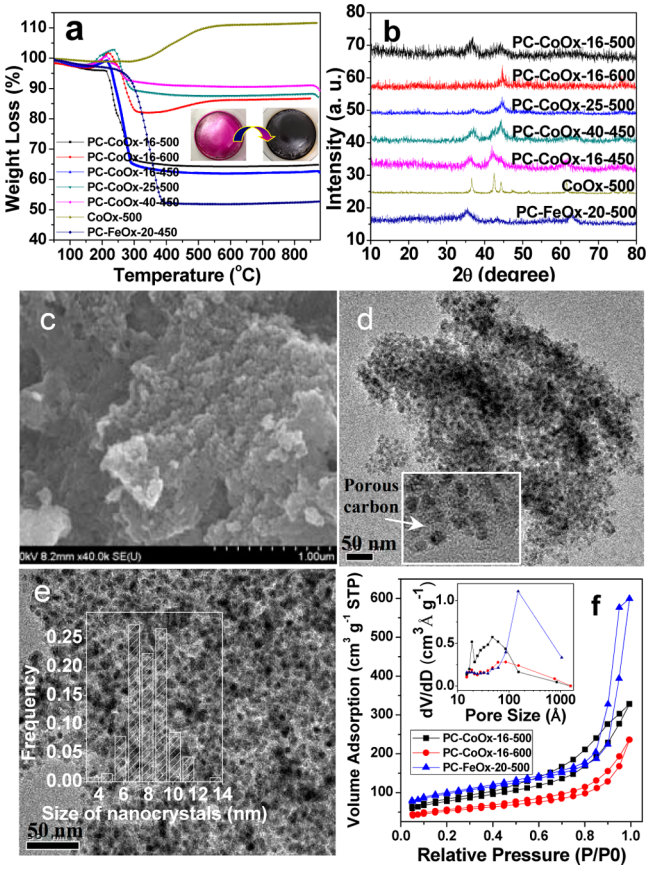

Figure 1. (a) TGA and (b) XRD patterns and of PC-CoO_x and PC-FeO_x. Inset of (a) is the digital picture of the solution conversion during the polymerization process in wide-mouth dish. SEM and TEM image of (c, d) PC-CoO_x-16−500 and (e) PC-CoO_x-16−600. Insets of d and e are enlargements of PC-CoO_x and the size distribution of CoO_x. (f) Nitrogen adsorption−desorption isotherms and pore size distribution of the PC-CoO_x and PC-FeO_x.

(CoO_x + C/H → Co + CO/CO_2 + H_2O; Co + O → CoO_x) changed based on the calcination temperature, therefore giving rise to varied CoO_x that with a low covalent. Even without carbon, direct decomposition of nitrate in Ar atmosphere also only produce CoO_x-500 powders, which lose a certain amount of oxygen from the lattices, as confirmed by the reoxidation process (weight increase of 12.1 wt %) within the temperature of 295−600 °C (Figure 1b). Because of the complex reactions existed in the materials under the inert atmosphere, composite oxides were often formed and herein acronymed as MO_x (e.g., CoO_x) simply. Thermalgrametric analysis (TGA) results show that the loading amount of metal oxide in PC-CoO_x composite could be readily tuned through varying the amount of metal oxide precursors and/or thermal conditions. For example, the weight losses, corresponding to the carbon mass percent in the samples of PC-CoO_x-16−450, 500, and 600, are about 38.1, 35.8, and 13.8%, demonstrating that enhancing the temperature could largely reduce the carbon content. Increasing the amount of precursor from 16 to 25 to 40 g, the mass percent of oxide increased from 64.2 to 87.6 to 90.6% and inevitably more amount of carbon could also be oxidized (CoO_x + C → CoO_y + CO/CO_2, $x > y$) during the carbonization. Noteworthy herein, it is necessary to decrease the calcination temperature below 500 °C when a high amount of precursor (e.g., >30 g) were used, such as 450 °C for PC-CoO_x-40, because the obtained CoO_x nanocrystals are so sensitive to air that the sample of PC-CoO_x could reburn after taking them out of the furnace even at room temperature if a high temperature was selected (e.g., 500 °C).

Scanning electron microscopy (SEM) image shows that the obtained materials are bulk without any regular morphology, which was determined by the similar sol−gel process (insets in panels a and c in Figure 1). However, the highly dispersive CoO_x nanocrystals with a narrow size distribution of 6 and 8 nm were well encapsulated in the porous carbon, as confirmed by the transmission electron microscopy (TEM) for the typical samples of PC-CoO_x-16−500 and 600 (Figure1d, e). BET results show that the composite have a high specific surface area of 268 and 178 $m^2\ g^{-1}$, together with the pore volume of 0.45 and 0.31 $cm^3\ g^{-1}$ respectively (Figure 1f). Herein, two kind of pores existed: one is the nanoporosity of carbon (<2 nm), which mainly resulted from the calcination of surfactants of F127, and the other is the mesoporosity (blank areas presented in the materials in panels d and in Figure 1, those consisting of the accumulation of PC-nanocrystals. The CoO_x nanocrystals encapsulated in the porous carbon (1−20 nm) could not only contact the outside moleculars/ions completely via rich porosity, but also could preserve their primary situations very well without any aggregation/collapse. Stimulating the intriguing properties of oxide nanocrystals, excellent conductivity of carbon and porous structure, this kind of materials were applied in the lithium-ion battery applications. Promisingly, the composite of PC-CoO_x-16−500 and 600 show ultrahigh performances. As shown in Figure 2a, the average

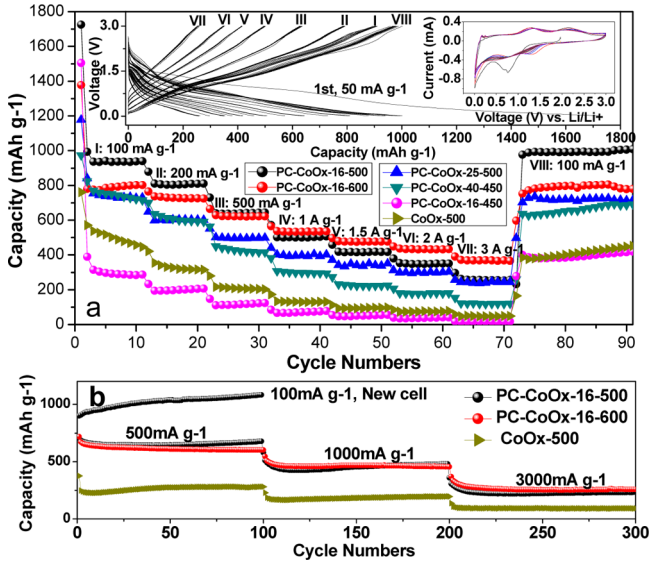

Figure 2. (a) Rate test of Li/PC-CoO_x cells under different current densities. Inset is the charge−discharge curves and cyclic voltammogram (CV). (b) Cycling performances of Li/PC-CoO_x.

capacity of PC-CoOx-16−500 could achieve as high as 937, 807, 640, 502 mA h g^{-1} (vs the mass of composite) at the current densities of 100, 200, 500, 1000 mA g^{-1}, respectively. These values are much higher than recent results of Co_3O_4/graphene (~800 mA h g^{-1} at 50 mA g^{-1}),[14] Co_3O_4/rGO (673 mA h g^{-1} at 180 mA g^{-1})[25] and Co_3O_4/CNTs (719 mA h g^{-1} at 200 mA g^{-1}).[26] Noteworthy, the mass percent of CoO_x in PC-CoO_x-500 is only about 64.2%, which means that the capacity versus CoO_x could achieve 1460, 1257, 997, 782 mA h

dx.doi.org/10.1021/am303178g | ACS Appl. Mater. Interfaces 2013, 5, 2133−2136

g^{-1}_{CoOx}. At the high current densities of 1.5, 2, and 3 A g^{-1}, the capacities of PC-CoO_x-16−600 are about 477, 434, 368 mA h g^{-1}, which shows better rate capability than those of PC-CoO_x-16−500 (417, 350, 256 mA h g^{-1}). This reason should be ascribed to the thinner carbon layer around of CoO_x nanocrystals in PC-CoO_x-16−600, which could largely facilitate the fast insertion/deinsertion of lithium ions.

However, considering the higher mass percent of CoO_x in PC-CoO_x-16−600 (86.2%) compare to that in PC-CoO_x-16−500 (64.2%), the capacities of PC-CoO_x-16−500 and 600 versus the mass of CoO_x are around 650, 545, 399 mA h g^{-1}_{CoOx}, and 553, 503, 427 mA h g^{-1}_{CoOx}, respectively at the current densities of 1.5, 2, and 3 A g^{-1}. Except a little lower capacity (versus the mass of CoO_x) at 3 A g^{-1}, the capacity of PC-CoO_x-16−500 are always higher than those of PC-CoO_x-16−600 (see Figure S1 in the Supporting Information). It clearly confirms that the utilization coefficient of CoO_x nanocrystal in PC-CoO_x-16−500 is much higher than that of CoO_x in PC-CoO_x-16−600. After the rate capability test, the capacities of PC-CoO_x-16−500 could recover back to 996 mA h g^{-1}, demonstrating the excellent recyclability of materials. The stable cycling performance was further confirmed by the cyclic voltammetry (Figure 2a, inset), and the peak around 0.7 V in the first cycle ascribed to the formation of solid electrolyte interface (SEI) on the surface of porous carbon surface.[27,28]

The poor performances of PC-CoO_x-16−450 (<400 m Ah g^{-1} even at 100 mA g^{-1}) discovered that the calcination temperature is a very important factor to determine the final properties of product (Figure 2a), even it also has cobalt oxide chemical composition as that in PC-CoO_x-16−500 (Figure 1b). Increasing the loading amount of oxide, the capacities of PC-CoO_x obviously changed. For example, the samples of PC-CoO_x-25−500 (87.6 wt %) and PC-CoO_x-40−450 (90.6 wt %) show capacities less than 800 mAh g^{-1} at a low current density of 100 mAh g^{-1} (Figure 2a). The reason probably ascribed to the instability of the sample taking out of the furnace and the varied crystalline phase of CoO_x after reoxidation in air, but which still need further investigation in detail. However, the performances of PC-CoO_x always show better performances than that of Co_3O_4-500 powders, except the sample of PC-CoO_x-16−450. It confirms that encapsulation of CoO_x nanocrystals into porous carbon is positive to enhance their properties; meanwhile, the amount of oxide and calcination temperature is the same critical to determine the final performances. Preliminary results demonstrate that the temperature between 500−600 °C and the oxide mass percent around 40−65% is beneficial to get a high performance. In this way, we could conclude that embedding CoO_x nanocrystals into porous carbon could largely enhance their utilization coefficient and then reduce the used amount of metal oxide in practical application.

The cycling performances of PC-CoO_x-16−500 and 600 were continually checked. As shown in Figure 2b, one new cell of Li/PC-CoO_x-16−500 shows a highly reversible capacity around 1021 mA h g^{-1} at the current density of 100 mA g^{-1} even after 100 cycles, demonstrating the excellent reproducibility of the materials. Moreover, the capacity of the used cell after rate test in figure 2a could still preserved around 654, 455, and 228 mA h g^{-1} after 100 cycles for each current density of 500, 1000, 3000 mA g^{-1} (Figure 2b). It fully confirms the stability of this kind of material with cycling more than 400 cycles. Under the same cycling conditions, the capacities of PC-CoO_x-16−600 are about 616, 464, and 262 mA h g^{-1}, which are much higher than 264, 182, and 93 mA h g^{-1} of CoO_x-500 powders (Figure 2b). From the viewpoint of the cost and utilization coefficient of CoO_x, the material of PC-CoO_x-16−500 shows the best performances among theses samples, even compare to PC-CoO_x-16−600, because its cycling capacity versus CoO_x are about 1019, 709, 355 mA g^{-1}_{CoOx} which are higher than those of PC-CoO_x-16−600 (714, 538, 304 mA g^{-1}_{CoOx}) (see Figure S2 in the Supporting Information).

Considering the high cost of cobalt in practical application and to confirm the feasibility of this presented strategy, we further prepared the composite of PC-FeO_x-20−500 and evaluated its electrochemical performances because of the low cost and high abundance of elemental Fe.[9,10,19,29]

TGA result of PC-FeO_x-20−500 shows that the mass percent of FeO_x was about 48.2%, and it has a large specific surface area of 329 m^2 g^{-1} and a pore volume of 0.83 cm^3 g^{-1}, in which the FeO_x nanocrystals with an average size distribution of 9.3 nm were highly dispersed (Figure 3a, b). Benefiting from this kind

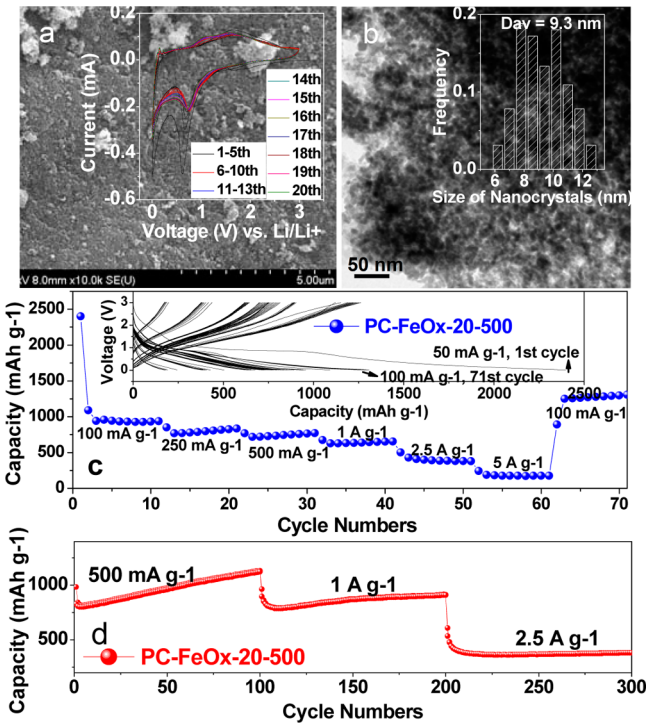

Figure 3. (a) SEM, (b) TEM image, (c) rate, and (d) cycling performances of PC-FeO_x-20−500. Insets pictures of a−c are the CV, histogram of nanocrystal size distribution, and rate charge−discharge curves, respectively.

of structure, the PC-FeO_x-20−500 also shows ultrahigh performances, such as highly reversible capacities of 937, 799, 743, 640, 394, 179 mA h g^{-1} at the current densities of 100, 250, 500, 1000, 2500, 5000 mA g^{-1} (Figure 3c). Meanwhile, the capacity of the cell could recover and increase to 1277 mA h g^{-1} at the current density of 100 mAh g^{-1} after the rate test (Figure 3c). These capacities of PC-FeO_x-20−500 are much higher than recent results of Fe_3O_4 particles (450 mA h g^{-1} at 185 mA g^{-1}),[10] Fe_3O_4/CF (~900 mA h g^{-1} at 100 mA g^{-1})[29] and RG-O/Fe_2O_3 composite (982 mA h g^{-1} at 100 mA g^{-1}).[30] The increase of stable capacity was also proved by the CV (from black over red to green curves, inset of Figure 3a) and it was ascribed to the activation of the metal oxide during the cycling. This phenomena of the capacity increased as the

dx.doi.org/10.1021/am303178g | ACS Appl. Mater. Interfaces 2013, 5, 2133−2136

cycling was also reported in the previous literature.[10−14] Ongoing research find that this kind of materials was well stabled in the continued cycling test (>300 cycles) even under the high current densities of 500, 1000, and 2500 mA g^{-1} with an average capacity of 976, 864, and 378 mAh g^{-1}, respectively (Figure 3d). Detail charge−discharge curves were provided in Figure S3 (see the Supporting Information).

CONCLUSION

Metal oxide nanocrystals with a high distribution were successfully encapsulated into the porous carbon via a simple and industrial scalable approach. In this way, the utilization coefficient of metal oxide could be largely enhanced while still preserving their intriguing properties, thereby achieving the goal of reducing the used amount of oxide in practical application. The synthetic conditions, including the appropriate loading amount of oxide and calcination temperature, were discussed in detail to facilitate its extension. With this method, the composite of PC-CoO_x and PC-FeO_x were prepared, and they show ultrahigh performances in lithium-ion battery. More importantly, this strategy of encapsulating metal oxide nanocrystals into porous carbon could be easily enlarged for the practical production, and a series of PC-metal (oxide) with high activities could be readily designed based on such general method for the widespread applications of catalysis, magnetic, sensor, fuel, and solar cell.

ASSOCIATED CONTENT

Supporting Information

Instrument and characterization, comparative capability of PC-CoO_x-16−500 and 600 versus the mass of CoO_x at rate and cycling test under different current densities, and discharge−charge curves of PC-FeO_x-20−500 during the cycling under the current densities of 500, 1000, 2500 mA g^{-1}. This information is available free of charge via the Internet at http://pubs.acs.org/.

AUTHOR INFORMATION

Corresponding Author

*E-mail: yksun@hanyang.ac.kr. Fax: +82 22282 7329. Tel: +82 2 2220.

Notes

The authors declare no competing financial interest.

ACKNOWLEDGMENTS

This work was supported by the Human Resources Development of the Korea Institute of Energy Technology Evaluation of Planning (KETEP) grant funded by the Korea government of Ministry of Knowledge Economy (20124010203310), and the National Research Foundation of KOREA (NRF) grant funded by the Korea government (MEST) (2009-0092780).

REFERENCES

(1) Lou, X. W.; Deng, D.; Lee, J. Y.; Feng, J.; Archer, L. A. *Adv. Mater.* **2008**, *20*, 258.
(2) Liu, J.; Xue, D. F. *Nanoscale Res. Lett.* **2010**, *5*, 1525−1534.
(3) Ji, L. W.; Lin, Z.; Alcoutlabi, M.; Zhang, X. W. *Energy Environ. Sci.* **2011**, *4*, 2682.
(4) Chae, C.; Kim, J. H.; Kim, J. M.; Sun, Y.-K.; Lee, J. K. *J. Mater. Chem.* **2012**, *22*, 17870.
(5) Liang, J.; Zhao, Y.; Guo, L.; Li, L. *ACS Appl. Mater. Interfaces* **2012**, *4*, 5742.
(6) Lou, X. W.; Archer, L. A.; Yang, Z. C. *Adv. Mater.* **2008**, *20*, 3987.
(7) Lou, X. W.; Chen, J. S.; Chen, P.; Archer, L. A. *Chem. Mater.* **2009**, *21*, 2868.
(8) Hu, Y. S.; Demir-Cakan, R.; Titirici, M. M.; Muller, J. O.; Schlogl, R.; Antonietti, M.; Maier, J. *Angew. Chem., Int. Ed.* **2008**, *47*, 1645.
(9) Zhang, L.; Wu, H. B.; Madhavi, S.; Hng, H. H.; Lou, X. W. *J. Am. Chem. Soc.* **2012**, *134*, 17388.
(10) Xu, J. S.; Zhu, Y. J. *ACS Appl. Mater. Interfaces* **2012**, *4*, 4752.
(11) Wen, W.; Wu, J. M. *ACS Appl. Mater. Interfaces* **2011**, *3*, 4112.
(12) Qiu, M. C.; Yang, L. W.; Qi, X.; Li, J.; Zhong, J. X. *ACS Appl. Mater. Interfaces* **2010**, *2*, 3614.
(13) Xia, X. H.; Tu, J. P.; Zhang, J.; Xiang, J. Y.; Wang, X. L.; Zhao, X. B. *ACS Appl. Mater. Interfaces* **2010**, *2*, 186−192.
(14) Wu, Z. S.; Ren, W. C.; Wen, L.; Gao, L. B.; Zhao, J. P.; Chen, Z. P.; Zhou, G. M.; Li, F.; Cheng, H. M. *ACS Nano* **2010**, *4*, 3187−3194.
(15) Ming, J.; Wu, Y.; Nagarajan, S.; Lee, D.-J.; Sun, Y.-K.; Zhao, F. *J. Mater. Chem.* **2012**, *22*, 22135.
(16) Lou, X. W.; Li, C. M.; Archer, L. A. *Adv. Mater.* **2009**, *21*, 2536.
(17) Liu, X.; Xie, K.; Wang, J.; Zheng, C. M.; Pan, Y. *J. Mater. Chem.* **2012**, *22*, 19621.
(18) Ko, S.; Lee, J. I.; Yang, H. S.; Park, S.; Jeong, U. *Adv. Mater.* **2012**, *24*, 4451.
(19) Latorre-Sanchez, M.; Primo, A.; Garcia, H. *J. Mater. Chem.* **2012**, *22*, 21373.
(20) Wang, H. L.; Cui, L. F.; Yang, Y. A.; Casalongue, H. S.; Robinson, J. T.; Liang, Y. Y.; Cui, Y.; Dai, H. J. *J. Am. Chem. Soc.* **2010**, *132*, 13978.
(21) Qiu, H.; Zou, F. *ACS Appl. Mater. Interfaces* **2012**, *4*, 1404.
(22) Ming, J.; Wu, Y.; Wang, L.; Yu, Y.; Zhao, F. *J. Mater. Chem.* **2011**, *21*, 17776.
(23) Ariga, K.; Vinu, A.; Yamauchi, Y.; Ji, Q.; Hill, J. P. *Bull. Chem. Soc. Jpn.* **2012**, *85*, 1.
(24) Merlet, C.; Rotenberg, B.; Madden, P. A.; Taberna, P.-L.; Simon, P.; Gogotsi, Y.; Salanne, M. *Nat. Mater.* **2012**, *11*, 306.
(25) Zhu, J.; Sharma, Y. K.; Zeng, Z.; Zhang, X.; Srinivasan, M.; Mhaisalkar, S.; Zhang, H.; Hng, H. H.; Yan, Q. *J. Phys. Chem. C.* **2011**, *115*, 8400.
(26) Zhuo, L.; Wu, Y.; Ming, J.; Wang, L.; Yu, Y.; Zhang, X.; Zhao, F. *J. Mater. Chem. A* **2013**, *1*, 1141.
(27) Novák, P.; Joho, F.; Lanz, M.; Rykart, B.; Panitz, J.-C.; Alliata, D.; Kötz, R.; Haas, O. *J. Power Sources.* **2001**, *97*−*98*, 39−46.
(28) Tang, M.; Miyazaki, K.; Abe, T.; Newman. *J. Electrochem. Soc.* **2012**, *159*, A634−A641.
(29) Yoon, T.; Chae, C.; Sun, Y.-K.; Zhao, X.; Kung, H. H.; Lee, J. K. *J. Mater. Chem.* **2011**, *21*, 17325.
(30) Zhu, X.; Zhu, Y.; Murali, S.; Stoller, M. D.; Ruoff, R. S. *ACS Nano* **2011**, *5*, 3333.